Holomorphic Embedding Model for Tracking Voltage Security Region Boundary of Power Systems

Menglei Zhi, Xue Li, Tao Jiang, Rufeng Zhang

Department of Electrical Engineering, Northeast Electric Power University, Jilin, China

{1202400011, xli, tjiang, zhangrufeng }@neepu.edu.cn

***Abstract*—The voltage security region (VSR) is a powerful tool for monitoring the voltage security of power systems with the influence of randomness and uncertain factors. To realize the accurate and fast construction of VSRs, a searching method for power system voltage security region boundary (VSR boundary, VSRB) based on holomorphic embedding method (HEM) is proposed. First, a holomorphic embedding (HE) searching model for a single VSRB point is proposed. A known operating point is set as the reference state, and the operating point at the security limit is set as the objective state. When the HE equations are solved at *s*=1, the solution is the next VSRB point. Such computation avoids the complex iterative process of continuation power flow (CPF) and significantly reduces the time cost. Secondly, to further enhance the computational efficiency of VSRB points, a boundary tracing strategy is introduced to enable the rapid search for adjacent boundary points. The VSRB can be formed by sequentially connecting the obtained boundary points. Finally, the accuracy and efficiency of the proposed method are analyzed and validated using IEEE-9 and IEEE-118 test systems. The results demonstrate that the proposed method can realize the accurate and fast construction of VSRB.**

***Index Terms* — Voltage security region, Voltage security region boundary, Holomorphic embedding, Continuation power flow**

I. INTRODUCTION

In response to the challenges posed by global warming and environmental degradation, the increasing integration of renewable energy has become an inevitable trend in the development of power systems. However, the high randomness and uncertainty of renewable energy sources, such as wind power and photovoltaics, pose significant challenges to the grid's voltage security [1]. The voltage security analysis of power system is generally based on simulation calculations under one or several fault scenarios defined by specified conditions, which is called the pointwise method [2]. However, the volatility of renewable energy output causes the actual power growth trajectory of the system to deviate from the preset direction, making it challenging for the pointwise method to accurately reflect the system's real-time operating status.

Furthermore, with the continuous expansion of the grid scale and the frequent occurrence of extreme events, multiple factors are influencing the voltage security of power systems. Such background necessitates the exploration of new approaches for voltage security analysis in multidimensional spaces. The voltage security region (VSR), a novel method for studying the voltage security of power systems, provides a comprehensive assessment of the system's multidimensional operating status [3]. It also illustrates the relationship between the system's current operating points and the voltage security boundary more intuitively. The accurate and rapid construction of VSR in power systems can be the basis for real-time voltage safety monitoring and preventing voltage-related emergency control events.

The foundation of constructing the VSR is to accurately and quickly identify the VSR Boundary (VSRB). All operating points within the VSRB are free from the risk of voltage violations, whereas those outside the VSRB cannot be operated safely [4]. VSRBs exhibit significant nonlinear characteristics, making it challenging to derive their analytical expressions directly. Existing studies typically construct mathematical expressions for the VSRB by searching for numerous VSRB points in the power injection space, followed by the application of fitting methods. Currently, some studies use continuation power flow (CPF) to search for VSRB points [5]. However, CPF-based VSRB points seeking requires extensive iterative processes to gradually approximate the optimal solution, making the solution process time-consuming and unfavorable for fast VSRB construction.

The holomorphic embedding method (HEM) offers a novel and efficient approach for solving nonlinear equations with certain conditions [6]. Based on complex analysis theory, HEM has been applied to power flow calculations. It embeds a complex variable s into the power flow equations and uses s to describe the system state transition from the reference state to objective state. When s equals to 0, the system is at the reference state and the holomorphic embedding (HE) equations should be easy to solve. When s is equal to 1, the system is at the objective state and the HE equations are equivalent to the original power flow equations. Based on the homotopy concept, this paper extends the HEM to the construction of the VSRB in power systems. The main contributions of this paper are as follows:

1) A searching model for a single VSRB point based on the HEM is proposed. Compared to the iterative process of CPF, the proposed method allows for direct and accurate searching of VSRB points.

2) The proposed HE-based VSRB boundary tracking model uses the parameters of the previously tracked VSRB point as the initial condition to explore the next adjacent point, which significantly improves the computational efficiency of VSRB.

This paper is structured as follows. Section II briefly introduces the concept and definition of VSR. Section III presents the HE models and specific computational steps for searching the VSRB using the HEM. Section IV analyzes and verifies the accuracy and efficiency of the proposed method using IEEE-9 and IEEE-118 test systems. Section V concludes the study.

II. DEFINITION OF VOLTAGE SECURITY REGION

The voltage security region of power systems is defined as the set of operating points in the active power injection space that satisfy both the power flow equations and the nodal voltage magnitude constraints. It is expressed as:

$$\Omega_U = \left\{ \boldsymbol{y} \left| \begin{array}{l} \boldsymbol{f}(\boldsymbol{x}, \boldsymbol{y}) = 0 \\ \max\left\{ U_i - U_i^{\max} \right\} \le 0, \forall i \in \Pi \\ \min\left\{ U_i - U_i^{\min} \right\} \ge 0, \forall i \in \Pi \end{array} \right. \right\} \tag{1}$$

where $\boldsymbol{f}$ denotes the system power flow equations; $\boldsymbol{x}$ and $\boldsymbol{y}$ represent the nodal voltage vector and the nodal power injection vector, respectively; Π denotes the set of all system nodes; U_i is the voltage magnitude at node i; and $U_i^{\max}$ and $U_i^{\min}$ denote the upper and lower voltage magnitude limits at node i, respectively.

979-8-3315-8138-1

When the system operates within the VSR defined in (1), all bus voltage magnitudes satisfy their upper and lower constraints. Directly searching for all voltage security operating points to construct the VSR is computationally prohibitive. Instead, the VSR can be found alternatively by identifying VSRB points, which substantially reduces the computational burden. As described in [7], the search model for VSRB points can be expressed as follows:

$$\begin{cases} \boldsymbol{f}(\boldsymbol{x},\boldsymbol{y})+\mu_1\boldsymbol{e}_1+\cdots+\mu_i\boldsymbol{e}_i+\cdots+\mu_N\boldsymbol{e}_N=0 \\ U_m=U_{\min}^{\text{set}} \text{ or } U_m=U_{\max}^{\text{set}} \end{cases} \tag{2}$$

where N denotes the number of system nodes; $\boldsymbol{e}_i$ represents an N-dimensional unit vector with a value of 1 at node i and 0 elsewhere (i = 1, 2, …, N); μ_i is the active power increment parameter for node i; and $U_{\max}^{\text{set}}$ and $U_{\min}^{\text{set}}$ denote the upper and lower voltage security limits at node m, respectively. By identifying the set of boundary points of the VSR, the boundary surface of the VSR can be constructed, enabling an intuitive and accurate assessment of the system's voltage security.

III. Searching for VSRB based on Holomorphic Embedding Method

The VSRB points model described in (2) can typically be solved using CPF. However, CPF involves extensive iterative computations, resulting in high computational burden and making them unsuitable for rapid VSRB construction. In contrast, the HEM exhibits continuity characteristics. By embedding a complex variable s into the VSRB equations and employing polynomial expansion and analytic continuation techniques, the complex VSRB solution problem is transformed into a continuous process of s from 0 to 1. This section presents a HE-based rapid search model for the VSRB and provides a detailed derivation of its solution procedure.

A. Framework of proposed VSRB search method

The diagram of the VSRB search method proposed in this paper is shown in Fig. 1. The proposed VSRB holomorphic embedding search model is:

$$\boldsymbol{\Phi}(\boldsymbol{z}(s))=\begin{cases} \boldsymbol{f}(\boldsymbol{x}(s),\boldsymbol{y})+\mu_1(s)\boldsymbol{e}_1+\cdots \\ +\mu_i(s)\boldsymbol{e}_i+\cdots+\mu_N(s)\boldsymbol{e}_N=0 \\ U_m(s)=U_{\min}^{\text{set}} \text{ or } U_m(s)=U_{\max}^{\text{set}} \end{cases} \tag{3}$$

where s denotes the embedded complex variable, and $\boldsymbol{z}(s)$= [$\boldsymbol{x}(s)$, $\mu_1(s)$, …, $\mu_N(s)$]$^{\mathrm{T}}$ represents the state variables after embedding s. $\boldsymbol{x}(s)$ is a column vector composed of the voltage phasors of all nodes. This section illustrates the fundamental procedure of the proposed voltage security boundary search method using the lower VSRB as an example.

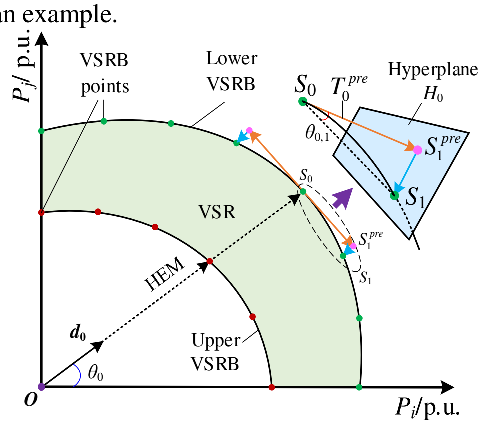

Fig. 1 Proposed VSRB boundary tracking strategy

The VSRB search illustrated in Fig. 1 consists of two steps. 1) For the first voltage security boundary point S_0, the search begins from the base operating state and proceeds along the specified power growth direction $\boldsymbol{d}_0$; 2) For subsequent boundary points, a boundary-tracking approach is adopted. Taking S_1 as an example. Starting from the previous boundary point S_0, the spatial correction tangent vector T_0^{pre} at S_0 is computed. Along this direction, a predicted point S_1^{pre} is obtained using a variable-step scheme. The next boundary point S_1 is then located along the spatial hyperplane perpendicular to the correction tangent vector. During the search process, only the first boundary point requires initialization from the base operating state. Subsequent boundary points are sequentially determined from adjacent points through tangent prediction and perpendicular correction steps. Evidently, the proposed method circumvents the complicated iterative process in CPF-based approaches, thereby significantly reducing the computation time for VSRB.

B. The HE-based initial VSRB point searching model

First, the HE searching model for the initial VSRB point constructed according to (3) is:

$$\boldsymbol{\Phi}(\boldsymbol{z}(s))=\begin{cases} \boldsymbol{f}(\boldsymbol{x}(s),\boldsymbol{y})+\lambda(s)\boldsymbol{d}_{\mathbf{0}}=0 \\ \boldsymbol{d}_{\mathbf{0}}=[\mu_1,\cdots,\mu_i,\cdots,\mu_N]^{\mathrm{T}} \\ U_m(s)-U_{\min}^{\text{set}}=0 \end{cases} \tag{4}$$

Where $\boldsymbol{d}_{\mathbf{0}}$=[$\mu_1$, …, μ_i, …,μ_N]$^{\mathrm{T}}$ represents the initial power growth direction, and μ_1, …, μ_N denote the initial power increments at each node, which are constant values. $\lambda(s)$ denotes the system load margin along the power growth direction $\boldsymbol{d}_0$ after embedding the complex variable s.

When searching for the first VSRB point, the process begins from the base operating state and proceeds along the power growth direction $\boldsymbol{d}_0$ using the HEM. Equation (4) is expanded to construct the HE equations corresponding to different node types as follows:

$$\begin{cases} \dot{U}_l^*(s^*)\sum_{k=1}^{N}Y_{l,k}\dot{U}_k(s)=S_{l,0}^*+s(S_l^*-S_{l,0}^*)+\lambda(s)\Delta P_l,\ l\in PQ \\ \mathrm{Re}(\dot{U}_p^*(s^*)\sum_{k=1}^{N}Y_{p,k}\dot{U}_k(s))=P_{p,0}+s(P_p-P_{p,0})+\lambda(s)\Delta P_p \\ \dot{U}_p(s)\dot{U}_p^*(s^*)=\dot{U}_{p,0}\dot{U}_{p,0}^*+s\left((U_p^{sp})^2-\dot{U}_{p,0}\dot{U}_{p,0}^*\right),\ p\in PV \\ U_r(s)=U_{r,0}+s(U_r^{sp}-U_{r,0}),\ r\in REF \\ \dot{U}_m(s)\dot{U}_m^*(s^*)=\dot{U}_{m,0}\dot{U}_{m,0}^*+s\left((U_m^{sp})^2-\dot{U}_{m,0}\dot{U}_{m,0}^*\right),\ m\in \Pi_{PQ} \end{cases} \tag{5}$$

where "Re" denotes the real part of a variable; "*" represents the complex conjugate operator; PQ, PV, REF, and Π_{PQ} denote the sets of load nodes, generator nodes, reference nodes, and concerned voltage security node, respectively; $Y_{l,k}$ represents the admittance between nodes l and k. S_l denotes the injected complex power at PQ node l; P_p denotes the injected active power at PV node p; ΔP_l and ΔP_p represent the active power increments at PQ node l and PV node p, respectively. $\dot{U}_l(s)$, $\dot{U}_p(s)$, $\dot{U}_r(s)$, and $\dot{U}_m(s)$ denote the HE functions of voltage phasors for PQ nodes, PV nodes, reference nodes, and the concerned voltage security node, respectively. U_p^{sp}, U_r^{sp} and U_m^{sp} denote voltage magnitudes of the PV node, reference node, and concerned voltage security node, respectively. $P_{p,0}$ denotes the initial injected reactive power at the PV node; $S_{l,0}$ denotes the initial injected complex power at the PQ node; $U_{p,0}$, $U_{r,0}$, and $U_{m,0}$ represent the initial voltage values of the PV node, reference node, and concerned voltage security node, respectively.

Expanding the unknown variables $\dot{U}_k(s)$ and $\lambda(s)$ in (5) using Taylor series:

$$\begin{cases} \dot{U}_k(s)=\sum_{n=0}^{\infty}a_{k,n}s^n \\ \lambda(s)=\sum_{n=0}^{\infty}\varsigma_n s^n \end{cases} \tag{6}$$

where k denotes the node index; $a_{k,n}$ represents the coefficient of the n-th term in the series expansion of the voltage phasor at node k; ς_n denotes the coefficient of the n-th term in the series expansion of the system load margin λ.

979-8-3315-8138-1

Substituting (6) into (5) and deriving the corresponding recursive relationships for the higher and lower order power series coefficients of the voltages and load margin:

$$\begin{cases} a_{l,0}^{*}\sum_{k=1}^{N}Y_{l,k}a_{k,n}+a_{l,n}^{*}\sum_{k=1}^{N}Y_{l,k}a_{k,0}-\varsigma_{n}\Delta P_{l}=\delta(n)(S_{l}^{*}-S_{l,0}^{*}) \\ -\beta(n)\sum_{q=1}^{n-1}a_{l,q}^{*}\sum_{k=1}^{N}Y_{l,k}a_{k,(n-q)},\ l\in PQ \\ \mathrm{Re}(a_{p,0}^{*}\sum_{k=1}^{N}Y_{p,k}a_{k,n}+a_{p,n}^{*}\sum_{k=1}^{N}Y_{p,k}a_{k,0})-\varsigma_{n}\Delta P_{p}= \\ \delta(n)(P_{p}-P_{p,0})-\beta(n)\mathrm{Re}\left(\sum_{q=1}^{n-1}a_{p,q}^{*}\sum_{k=1}^{N}Y_{p,k}a_{k,(n-q)}\right) \\ a_{p,0}^{*}a_{p,n}+a_{p,n}^{*}a_{p,0}=-\beta(n)\sum_{q=1}^{n-1}a_{p,q}^{*}a_{p,(n-q)},\ p\in PV \\ a_{r,n}=\delta(n)(U_{r}^{sp}-U_{r,0}),\ r\in REF \\ a_{m,0}^{*}a_{m,n}+a_{m,n}^{*}a_{m,0}=-\beta(n)\sum_{q=1}^{n-1}a_{m,q}^{*}a_{m,(n-q)},\ m\in \Pi_{PQ} \end{cases} \tag{7}$$

Where $\delta(n)$ and $\beta(n)$ are

$$\delta(n)=\begin{cases}1 & ,n=1\\ 0 & ,n>1\end{cases},\ \beta(n)=\begin{cases}0 & ,n=1\\ 1 & ,n>1\end{cases}$$

Using (7), the coefficients $a_{k,n}$ and ς_n in (6) can be determined. Subsequently, applying the Padé approximation to (6) and setting s=1 yields the solutions of $\dot{U}(s)$ and $\lambda(s)$ at the VSRB points:

$$x_i^n(s)=\sum_{k=0}^{L}d_{i,k}s^k \Big/ \sum_{k=0}^{M}b_{i,k}s^k \tag{8}$$

Where $x_i^n(s)$ represents the state variables to be approximated, n represents the number of terms of the power series, with $n=L+M$. The coefficients $d_{i,k}$ and $b_{i,k}$ are derived from the known power series, and then substituting s=1 yields the numerical value of the state variable x_i.

C. The HE-based VSRB boundary tracking model

After obtaining the first VSRB point, the subsequent VSRB points are identified using a boundary-tracking approach. The proposed method first constructs the spatial tangent vector at the previous boundary point, then obtains the predicted boundary point in the tangent direction, and finally acquires the actual VSRB point along the direction perpendicular to the tangent vector. The specific search model is as follows.

1) Construct the spatial tangent vector at the boundary point $S_{k\text{-}1}$.

Taking the lower boundary as an example, the VSRB boundary tracking search model from $S_{k\text{-}1}$ to S_k is formulated based on (3).

$$\boldsymbol{\Phi}(z(s))=\begin{cases}\boldsymbol{f}(\boldsymbol{x}(s),\boldsymbol{y})+\lambda_{k-1}\boldsymbol{d}_{k-1}+\mu_i(s)\boldsymbol{e}_i+\mu_j(s)\boldsymbol{e}_j=0\\ U_m(s)-U_{\min}^{\text{set}}=0\end{cases} \tag{9}$$

where $\lambda_{k\text{-}1}$ and $\boldsymbol{d}_{k\text{-}1}$ denote the load margin and power growth direction at the previous boundary point $S_{k\text{-}1}$, respectively.

The spatial tangent vector $T_{k\text{-}1}$ at the VSRB point $S_{k\text{-}1}$ is

$$T_{k-1}=\begin{bmatrix}\dfrac{\partial \boldsymbol{f}(\boldsymbol{x}_{k-1}(s))}{\partial \boldsymbol{x}} & \boldsymbol{e}_i & \boldsymbol{e}_j\\ \dfrac{\partial (U_m(s)-U_{\min}^{\text{set}})}{\partial \boldsymbol{x}} & 0 & 0\\ \boldsymbol{0} & 0 & 1\end{bmatrix}^{-1} E \tag{10}$$

where E= [0, …, 0, τ]$^{\mathrm{T}}$. When τ= 1, $T_{k\text{-}1}$ points toward the direction of increasing power angle; when τ= −1, $T_{k\text{-}1}$ points toward the direction of decreasing power angle. In the search process from S_0 to S_1 shown in Fig. 1, τ= −1.

2) Calculate the nodal voltages at the prediction point S_k^{pre} and the corrected tangent vector $T_{k\text{-}1}^{pre}$.

$$\begin{cases}z_k^{pre}=z_{k-1}+\sigma\cdot \overline{T}_{k-1}\\ \sigma=\sqrt{\dfrac{2\varepsilon_{tol}}{\kappa}}\end{cases} \tag{11}$$

where σ denotes the prediction step size, ε_{tol} denotes the allowable prediction error tolerance, κ represents the curvature at the preceding boundary point, and $\overline{T}_{k\text{-}1}$ represents the normalized spatial tangent vector. Based on (11), the power injection and node voltage information at the predicted point S_k^{pre} can be obtained. Since the tangential prediction deviates from the original power flow equations, discrepancies arise between the calculated voltages and the corresponding injected powers. Using the power at the predicted point S_k^{pre} as the target value and the voltage at S_0 as the initial condition, the actual node voltages $\dot{\boldsymbol{U}}_k^{pre}$ at S_k^{pre} can be obtained from (5). Subsequently, the corrected tangent vector $T_{k\text{-}1}^{pre}$ is derived based on z_k^{pre} and z_{k-1}:

$$T_{k-1}^{\text{pre}}=\sigma\cdot\frac{z_k^{pre}-z_{k-1}}{\left|z_k^{pre}-z_{k-1}\right|} \tag{12}$$

3) Search for boundary point S_k along the direction perpendicular to the tangent vector $T_{k\text{-}1}^{pre}$.

Based on the orthogonality between the hyperplane $H_{k\text{-}1}$ and the corrected tangent vector $T_{k\text{-}1}^{pre}$, the following relationship holds:

$$\begin{aligned}T_{k-1}^{pre}\cdot(z_k-z_{k-1})^{\mathrm{T}}&=\left|T_{k-1}^{pre}\right|\cdot\left|z_k-z_{k-1}\right|\cos\theta_{k-1,k}\\ &=\sigma\left|\overline{T}_{k-1}^{pre}\right|\cdot\left|z_k-z_{k-1}\right|\cdot\frac{\left|T_{k-1}^{pre}\right|}{\left|z_k-z_{k-1}\right|}=\sigma\left|T_{k-1}^{pre}\right|\end{aligned} \tag{13}$$

By combining (9) and (13), the boundary point S_k can be determined as following steps:

(a) Derive the recursive relationship for the coefficients of the power series.

The active power balance equations for the coordinate axis nodes i and j are given by:

$$\begin{cases}\mathrm{Re}(\dot{U}_i^*(s^*)\sum_{k=1}^{N}Y_{i,k}\dot{U}_k(s))-P_{i,k}^{\text{pre}}-\mu_i(s)=0\\ \mathrm{Re}(\dot{U}_j^*(s^*)\sum_{k=1}^{N}Y_{j,k}\dot{U}_k(s))-P_{j,k}^{\text{pre}}-\mu_j(s)=0\end{cases} \tag{14}$$

where $P_{i,k}^{pre}$ and $P_{j,k}^{pre}$ denote the active power injections at nodes i and j at the preceding boundary point S_k^{pre}, respectively. Expanding each variable in (14) into a power series yields the recursive relationships between the n-th order power series coefficients and the lower-order terms:

$$\begin{cases}\mathrm{Re}(a_{i,0}^{*}\sum_{k=1}^{N}Y_{i,k}a_{k,n}+a_{i,n}^{*}\sum_{k=1}^{N}Y_{i,k}a_{k,0})-\mu_{i,n}\\ \quad=-\mathrm{Re}\left(\sum_{q=1}^{n-1}a_{i,q}^{*}\sum_{k=1}^{N}Y_{i,k}a_{k,(n-q)}\right)\\ \mathrm{Re}(a_{j,0}^{*}\sum_{k=1}^{N}Y_{j,k}a_{k,n}+a_{j,n}^{*}\sum_{k=1}^{N}Y_{j,k}a_{k,0})-\eta_{j,n}\\ \quad=-\mathrm{Re}\left(\sum_{q=1}^{n-1}a_{j,q}^{*}\sum_{k=1}^{N}Y_{j,k}a_{k,(n-q)}\right)\end{cases} \tag{15}$$

Except for the HE equations of active power balance at nodes i and j, the HE equations for all other nodes follow the same form as (5), and their recursive relationships are similar to those in (7).

The HE equation of (13) is:

$$T_{k-1}^{pre}\cdot(z_k(s)-z_{k-1})^{\mathrm{T}}=\sigma\left|T_{k-1}^{pre}\right| \tag{16}$$

Similarly, expanding the holomorphic function in (16) into a power series yields the following recursive relationship:

$$\sum_{l=1}^{N}(a_l^{T_{pre,k-1}}a_{l,n})+\mu_i^{T_{pre,k-1}}\mu_{i,n}+\eta_j^{T_{pre,k-1}}\eta_{j,n}=0 \tag{17}$$

where $a_l^{T_{pre,k-1}}$ denotes the voltage phasor of node l in the corrected tangent vector $T_{k\text{-}1}^{pre}$; $\mu_l^{T_{pre,k-1}}$ and $\eta_l^{T_{pre,k-1}}$ represent the active power increment parameters of nodes i and j in $T_{k\text{-}1}^{pre}$, respectively; $\mu_{i,n}$ and $\eta_{j,n}$ denote the n-th order power series coefficients of the active power increments for nodes i and j at the boundary point S_k, respectively.

(b) Solve the HE equations of VSRB points.

Equations (7), (15), and (17) can be collectively expressed as:

$$AX[n] = RHS \tag{18}$$

Where $X[n]$ represents the n-th order power series coefficients of the voltage and power increments, including $a_{k,n}$, $\mu_{i,n}$ and $\eta_{j,n}$; A is the core computational matrix composed of state variables at the predicted boundary point and the system admittance matrix. A remains constant throughout the computation, while RHS represents the power series coefficients of the unknown variables of orders lower than n. When solving for $X[n]$, RHS is always known. In each recursive step, only the RHS values are updated to obtain $X[n]$. After computing $X[n]$, the solutions of the voltage and power increments are derived using the Padé approximation in (8), thereby determining the quantities at the VSRB point.

After locating the adjacent boundary point S_k from S_{k-1} using the proposed HE-based boundary tracking method, the same search process is repeated with S_k as the new starting point until all voltage security boundary points within the lower half-plane of the $\boldsymbol{d}_0$ search direction in the first quadrant are identified. The search is then restarted from S_0 to locate the VSRB points in the upper half-plane. After searching the lower VSRB boundary points, the upper boundary points are obtained using the same procedure, except that the voltage magnitude of the concerned voltage security node is set to $U_{\max}^{\text{set}}$.

4) Construct the VSRB using VSRB points.

After completing the search for VSRB points in the first quadrant, the lower VSRB points are sequentially connected to form the lower boundary of the VSR. The upper boundary can be constructed in the same way. Once upper and lower VSRBs are obtained, the VSR in the 2D active power injection space is acquired. The three-dimensional VSRB can be obtained by fitting multiple two-dimensional VSRB. The detailed solution procedure is provided in [7].

Discussions: The proposed method explicitly accounts for generator reactive power limit violations. Taking the search for the initial boundary point as an example, the procedure is as follows: After obtaining a boundary point, verify whether the generator's reactive power output violates its limits. If a violation occurs, switch the corresponding PV bus to PQ bus and recompute the boundary point following Section III-B. Repeat this procedure until no generator violates its reactive power limits.

IV. Case Study

In this section, the performance of the proposed HEM for searching the VSRB in the 2D and 3D space is evaluated with the IEEE-9 test system and the IEEE-118 test system [8]. The power base is set to 100 MVA, and the upper and lower security limits of the nodal voltage magnitude are set to 1.05 p.u. and 0.95 p.u., respectively.

A. *IEEE-9 test system*

The VSRB of bus 5 is searched by using the proposed HEM with the active power injection from buses 5 and 9 selected as the axis. Fig. 2 presents the search results of the proposed method. Taking the lower VSRB as an example, the detailed search process is as follows.

First, starting from the coordinate origin, the boundary point S_0 is searched using the HE-based initial VSRB point searching model. The initial power grid stress direction is given as $\boldsymbol{d}_0$=[0, 0, 0, 0, 0.5843, 0, 0, 0, 0.8115]$^{\mathrm{T}}$, and the HE model is established based on (5). When the voltage power series expansion order reaches 16, the voltage magnitude of bus 5 obtained from (8) is 0.9500p.u. At this point, the maximum system power mismatch is 7.5897×10^{-6}p.u, which is less than the specified tolerance of 1×10^{-5}p.u. The search for the first boundary point S_0 has been completed with coordinates (1.5949, 2.2027).

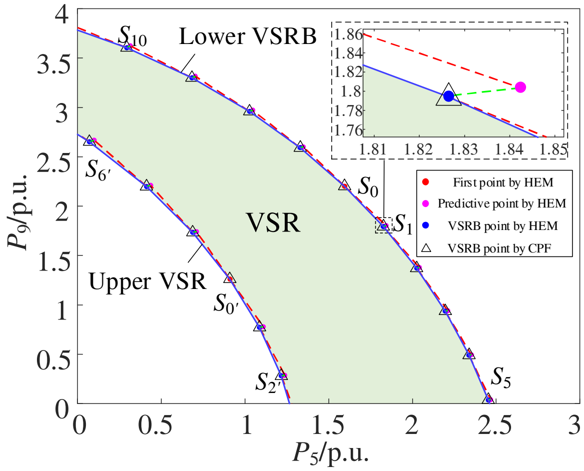

Fig. 2 2D VSRB of IEEE-9 test system

After obtaining the first boundary point S_0, the next boundary point S_1 is determined using the proposed HE-based VSRB boundary tracking model. First, the voltage values at point S_0 is used as the initial solution for the HE-based VSRB equation (9), and the unit vectors $\boldsymbol{e}_5$ and $\boldsymbol{e}_9$ are specified. Set $\tau= -1$ and based on (10), the tangent vector T_0 at the boundary point is obtained, and the predicted point S_1^{pre} is determined with coordinates (1.8424, 1.8035). The corrected tangent vector T_0^{pre} is derived from (11) and (12), and the power series coefficients of the voltage and power increments are obtained from (18). When the expansion order reaches 2, the voltage magnitude at node 5 obtained from (8) is 0.9500 p.u. At this point, the maximum system power mismatch is 3.2538×10^{-7}p.u., which is smaller than the specified tolerance. The search for the first boundary point S_1 has been completed, with coordinates (1.8260 ,1.7948). Then, starting from boundary point S_1, boundary point S_2 is located using a procedure analogous to that employed for S_1. This process is repeated until the coordinate of a boundary point becomes less than zero, at which point the downward search is terminated. Subsequently, starting from boundary point S_0, boundary points in the upper half-plane are searched using the proposed HE-based VSRB boundary tracking model. Unlike the lower half-plane case, τ=−1 in (10) during this stage.

TABLE I

Coordinates and errors of VSRB points of WECC-9 test system

NO.	VSRB point coordinates obtained by HEM	Absolute error/p.u.		NO.	VSRB point coordinates obtained by HEM	Absolute error/p.u.	
		HEM	CPF			HEM	CPF
S_0	(1.5949, 2.2027)	3.0816E-15	2.2204E-16	S_{10}	(0.2941, 3.6051)	1.6568E-15	4.4409E-16
S_1	(1.8260, 1.7948)	2.2204E-16	1.1102E-16	S_{11}	(-0.1384, 3.8659)	1.1635E-14	3.3307E-16
S_2	(2.0254, 1.3723)	1.4943E-15	2.2204E-16	$S_{0'}$	(0.9095, 1.2615)	1.5473E-13	6.6613E-16
S_3	(2.1956, 0.9373)	1.1102E-16	1.1102E-16	$S_{1'}$	(1.0864, 0.7723)	1.7741E-15	2.2204E-16
S_4	(2.3378, 0.4918)	9.0242E-15	3.3307E-16	$S_{2'}$	(1.2165, 0.2821)	1.3746E-15	2.2204E-16
S_5	(2.4527, 0.0381)	7.6943E-15	1.1102E-16	$S_{3'}$	(1.3023, -0.2077)	1.2632E-14	1.1102E-16
S_6	(2.5407, -0.4214)	6.9563E-15	3.3307E-16	$S_{4'}$	(0.6877, 1.7350)	1.9574E-14	3.3307E-16
S_7	(1.3295, 2.5928)	3.1655E-14	3.3307E-16	$S_{5'}$	(0.4117, 2.1999)	3.0634E-14	1.1102E-16
S_8	(1.0269, 2.9601)	5.5734E-14	2.2204E-16	$S_{6'}$	(0.0710, 2.6524)	5.5568E-14	1.1102E-16
S_9	(0.6829, 3.2999)	1.1643E-15	2.2204E-16	$S_{7'}$	(-0.3492, 3.0846)	1.2642E-15	1.1102E-16

After completing the lower VSRB points search, the adjacent boundary points are sequentially connected to form the upper VSRB. The search process for the upper VSRB follows the same procedure, except that the voltage security limit is set to 1.05 p.u. Once all the critical points on the VSRB are obtained, the VSR for bus 5 in the 2D active power injection space is acquired.

The detailed information of the VSRB points on the upper and lower VSRBs are listed in Table I. The results in Table I show that the minimum absolute error of the VSRB points calculated by the proposed method is 1.1102×10^{-16} p.u., while the maximum absolute error is only 1.5473×10^{-13} p.u., thereby verifying the high computational accuracy of the proposed method.

Furthermore, the proposed HEM is employed to search for 3D VSRBs. Fig. 3 shows the tracked VSRB of bus 9 with the active power injection from buses 5, 7, and 9 selected as the axis.

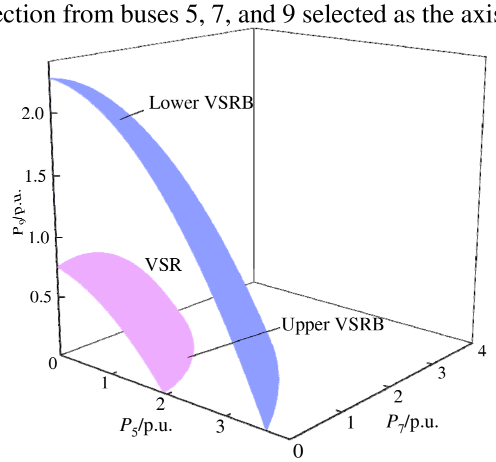

Fig. 3 3D VSRB of IEEE-9 test system

Fig. 4 further quantifies the absolute error range of the 89 VSRB points obtained by the proposed HEM in 3D active power injection space. The results indicate that 71.91% of the VSR boundary points exhibit absolute errors below 1×10^{-14} p.u., while the error of only 25 boundary points fall within the range of 1×10^{-14} p.u to 1×10^{-6} p.u. The results demonstrate that the proposed method achieves high accuracy in constructing 3D VSRBs.

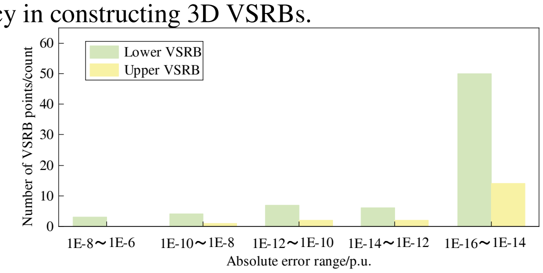

Fig.4 Histogram of errors of VSRB points of IEEE-9

B. *IEEE-118 test system*

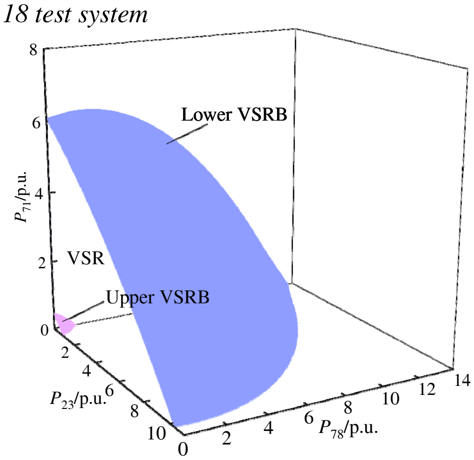

Fig. 5 3D VSRB of IEEE-118 test system

In this section, the proposed VSRB searching approach is implemented on the IEEE-118 test system to evaluate its effectiveness and performance in bulk power systems. Fig. 5 shows the tracked VSRB of bus 75 with the active power injection from buses 23, 71, and 78 selected as the axis. In this case, the maximum absolute error of the VSRB point is only 7.6353×10^{-10}p.u. The results demonstrate that the proposed HEM also achieves high accuracy in constructing VSRBs for bulk power systems. Furthermore, the 3D VSRB are projected onto 2D active power injection spaces, as shown in Fig. 6.

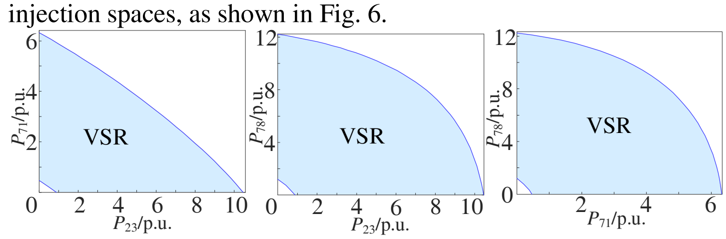

Fig. 6 2D VSRB of IEEE-118 test system

C. *Computational efficiency*

Table II further compares the computation times of the proposed HEM and the CPF method for searching 2D and 3D VSRBs in the IEEE-9 and IEEE-118 test systems. As shown in the Table II, the HEM-based VSRB constructing approach achieves over 65% higher computational efficiency compared with the CPF method.

TABLE II

COMPUTATIONAL TIMES OF IEEE-9 AND IEEE-118 TEST CASES

Test system	Concerned voltage security node	Power injection bus	HEM/s	CPF/s	Improvement
IEEE-9	5	5, 9	0.3012	0.9573	68.54%
	9	5, 7, 9	1.1264	3.7432	69.91%
IEEE-118	75	23, 71	0.3453	1.4318	75.88%
	75	23, 78	0.4143	1.5632	73.50%
	75	71, 78	0.3853	1.3942	72.36%
	75	23, 71, 78	7.0481	21.5352	67.27%

V. CONCLUSION

This paper proposes a HE-based method to construct the VSRB for power systems. The performance of the proposed approach is validated by the case studies on the IEEE-9 test system and the IEEE-118 test system. The results demonstrate that the proposed method enables high-precision and efficient construction of VSRBs. The proposed method significantly improves power systems voltage security monitoring capability, providing grid operators with accurate and practical tools for voltage security analysis.

ACKNOWLEDGEMENT

The work is supported by the National Natural Science Foundation of China (Grant No. 52577088).

REFERENCES

[1] J. Li, Z. B. Qin, and Y. C. Luo, "Research on future trends of electricity consumption based on conditional generative adversarial network considering dual-carbon target," *IET Energy Syst. Integr*., vol. 6, no. 4, pp. 437-450, Feb. 2024.

[2] T. Ding, R. Bo, and H. Sun, "A Robust Two-Level Coordinated Static Voltage Security Region for Centrally Integrated Wind Farms," *IEEE Trans. Smart Grid*, vol. 7, no. 1, pp. 460-470, Jan. 2016.

[3] H. D. Nguyen, K. Dvijotham, and K. Turitsyn, "Constructing convex inner approximations of steady-state security regions," *IEEE Trans. Power Syst*., vol. 34, no. 1, pp 257-267, Jan. 2019.

[4] Y. Qiu, H. Wu, and Y. Zhou, "Global parametric polynomial approximation of static voltage stability region boundaries," *IEEE Trans. Power Syst*., vol. 32, no. 3, pp 2362-2373, May. 2017.

[5] V. Ajjarapu and C. Christy, "The continuation power flow: a tool for steady state voltage stability analysis," *IEEE Trans. Power Syst*., vol. 7, no. 1, pp. 416-423, Feb. 1992.

[6] S. Rao, F. Yang, and D. J. Tylavsky, "The holomorphic embedding method applied to the power-flow problem," *IEEE Trans. Power Syst*., vol. 31, no. 5, pp 3816-3828, Sept. 2016.

[7] X. Li, L. W. Zhang, and T. Jiang, "Relaxed decoupled direct calculation of voltage collapse points and its application in static voltage stability region boundary formation," *Int. J. Electr. Power Energy Syst.*, vol. 125, Feb. 2021, Art. no. 106452.

[8] R. D. Zimmerman, C. E. Murillo-Sánchez, and R. J. Thomas, "MATPOWER: Steady-state operations, planning, and analysis tools for power systems research and education," *IEEE Trans. Power Syst*., vol. 26, no. 1, pp 12-19, Feb. 2011.

979-8-3315-8138-1